



1 **Evaluation of cloud effects on air temperature estimation using MODIS LST**

2 **based on ground measurements over the Tibetan Plateau**

3 Hongbo Zhang^{1,2}, Fan Zhang^{1,2}, Guoqing Zhang^{1,2}, Xiaobo He³, Lide Tian^{1,2}

4 ¹Key Laboratory of Tibetan Environment Changes and Land Surface Processes, Institute of
5 Tibetan Plateau Research, Chinese Academy of Sciences, Beijing, China

6 ²CAS Center for Excellence in Tibetan Plateau Earth Sciences, Beijing, China

7 ³Cold and Arid Regions Environmental and Engineering Research Institute, Chinese Academy of
8 Sciences, Lanzhou, China

9

10

11

12

13 *Correspondence to:* Hongbo Zhang, Tel.: +86-10-84097030; fax: +86-10-84097079.

14 E-mail address: zhanghongbo@itpcas.ac.cn

15

16

17

18 **Abstract**

19 Moderate Resolution Imaging Spectroradiometer (MODIS) land surface temperature (LST) data
20 have played a significant role in estimating the air temperature (T_{air}) due to the sparseness of
21 ground measurements, especially for remote mountainous areas. Generally, two types of air
22 temperatures are studied including daily maximum (T_{max}) and minimum (T_{min}) air temperatures.
23 MODIS daytime and nighttime LST are often used as proxies for estimating T_{max} and T_{min} ,
24 respectively. The Tibetan Plateau (TP) has a high daily cloud cover fraction (>45%). The presence
25 of clouds can affect the relationship between T_{air} and LST and can further affect the estimation
26 accuracies. This study comprehensively analyzes the effects of clouds on T_{air} estimation based on
27 MODIS LST using detailed half-hourly ground measurements and daily meteorological station
28 observations collected from over the TP. Comparisons made between in-situ cloudiness
29 observations and MODIS claimed clear-sky records show that erroneous rates of MODIS
30 nighttime cloud detection are obviously higher than those achieved in daytime. Our validation of
31 the MODIS LST values under different cloudiness constraining conditions shows that the
32 accuracy of MODIS nighttime LST is severely affected by undetected clouds. Large errors
33 introduced by undetected clouds are found to significantly affect the T_{min} estimations based on
34 nighttime LST through cloud effect tests. However, clouds are mainly found to affect T_{max}
35 estimation by affecting the essential relationship between T_{max} and daytime LST. The obviously
36 larger errors of T_{max} estimation than those of T_{min} could be attributed to larger MODIS daytime
37 LST errors resulting from higher degrees of daytime LST heterogeneity within MODIS pixel than
38 those of nighttime LST. Constraining all four MODIS observations per day to non-cloudy
39 observations can efficiently screen samples to build a strong fit of T_{min} estimation using MODIS
40 nighttime LST. The present study reveals the effects of clouds on T_{air} estimation through MODIS
41 LST and will thus help improve the estimation accuracy levels while alleviating the problems
42 associated with severe data sparseness over the TP.

43

44 **Keywords:** cloud effects, MODIS LST, air temperature estimation, Tibetan Plateau

45



46 **1 Introduction**

47 Air temperature is a key variable used to describe environmental conditions. However,
48 temperature observations are typically sparse in remote mountainous areas (Lin et al., 2016).
49 Remotely sensed land surface temperatures (LST) can serve as an efficient proxy for air
50 temperature estimation in such areas. Superior to limited ground measurements, remote sensing
51 can provide more spatiotemporal information. Several studies have estimated air temperatures
52 using Moderate Resolution Imaging Spectroradiometer (MODIS) land surface temperature
53 products for Europe (Kilibarda et al., 2014; Benali et al., 2012), Canada (Xu et al., 2014), USA
54 (Oyler et al., 2016; Oyler et al., 2015; Parmentier et al., 2015), Africa (Vancutsem et al., 2010; Lin et
55 al., 2012), western Asia (Emamifar et al., 2013) and the Tibetan Plateau (TP) (Zhu et al., 2013; Fu
56 et al., 2011).

57 Due to its high altitudes, the TP includes the largest cryosphere area outside the Arctic and
58 Antarctic regions and outside Greenland, and it is considered to be among the areas that are most
59 sensitive to climate change. However, most meteorological stations in the TP are located in
60 low-altitude (< 4800 m) and eastern regions (Fig. 1). There are almost no stations in the vast
61 western area or at the elevations above 5000 m. In particular, for glacier covered areas,
62 temperature observations are extremely scarce (Wu et al., 2015). Remotely sensed LSTs can
63 greatly help alleviate the problems associated with scarce temperature observations available for
64 the TP.

65 Despite the advantages of high spatial and temporal accessibility to large-scale areas, remote
66 sensing data present some limitations, among which cloud contamination issues may be the most
67 important. For applications of MODIS LST, clouds can affect the T_{air} estimation in at least two
68 ways: erroneous cloud identification can reduce the accuracy of MODIS LST values, and the
69 presence of clouds can affect the relationship between LST and T_{air} and can further affect the
70 accuracy of T_{air} estimations.

71 The presence of clouds can greatly decrease the amount of data available in the satellite images.
72 Moreover, the existing cloud detection algorithms cannot identify all the cloudy pixels, and a
73 considerable percentage of undetected cloudy pixels exists in MODIS LST products (reported at
74 roughly 15%) (Ackerman et al., 2008). It has been shown through some validation studies that
75 extremely large differences (>10 K) between MODIS LST and ground measurements occasionally



76 occur, even for homogeneous surfaces. In these cases, the cloud top temperatures can be taken as
77 the LST values (Langer et al., 2010; Westermann et al., 2011). More recently, up to 40% of ground
78 measured cloudy samples have been labeled unidentified according to field observations, thus
79 producing rather large MODIS LST errors, as reported for Svalbard (Østby et al., 2014). Such
80 errors can disturb the true relationship between LST and air temperatures (T_{air}). MODIS daytime
81 LST has been found to be affected by unidentified cloudy pixels, causing such pixels to severely
82 degrade LST- T_{air} relationships (Williamson et al., 2013). Because the daytime cloud algorithm is
83 expected to present more confidence than that for nighttime (Ackerman et al., 1998), using the
84 nighttime LST for air temperatures may be influenced more by undetected clouds. For the TP,
85 cloud contamination also constitutes a major problem, generating a mean daily cloud cover
86 fraction of $> 45\%$ (Yu et al.). Thus, the effects of clouds are particularly essential for T_{air}
87 estimation in the TP.

88 In addition to the effects of undetected cloudy pixels, clouds are expected to play a key role in the
89 relationship between LST and T_{air} due to its cooling effects during the day and warming effects at
90 night (Dai et al., 1999). During the day, clouds can decrease land surface warming rates by
91 blocking solar radiation, and at night, clouds can reflect surface long wave radiation and decrease
92 heat losses from the land surface producing higher ground temperatures than those detected on
93 clear days. For example, the difference between observed daytime LST and T_{air} under cloudy
94 conditions is much lower (an average of $\sim 3.7^\circ\text{C}$) than that observed under clear conditions (Gallo
95 et al., 2011). Therefore, questions regarding whether and how clouds can affect relationships of
96 T_{max} -Daytime LST and T_{min} -Nighttime LST have been posed. Previous T_{air} estimation based on
97 MODIS LST are presumably valid for clear conditions (Shen and Leptoukh, 2011; Oyler et al.,
98 2015). However, satellite observed LSTs (in night or day) are instantaneous and may have a time
99 lag between the overpass time and the time when T_{air} reaches its minimum or maximum. Daily
100 cloudiness conditions may affect the warming (during the day) or cooling (at night) rates and can
101 further alter the relationship between T_{air} and LST.

102 Previous studies have mainly focused on two types of daily T_{air} estimations: daily maximum (T_{max})
103 and minimum (T_{min}) air temperatures (Xu et al., 2014; Benali et al., 2012; Good, 2015). In addition,
104 daytime and nighttime LST have been used as predictors for T_{max} and T_{min} estimations,
105 respectively, due to their different overpass times (Vancutsem et al., 2010; Lin et al., 2012; Oyler et



106 al., 2016). Recent studies have interestingly found that the estimation accuracy of T_{\max} based on
107 daytime LST is clearly lower than that of T_{\min} based on nighttime LST (Oyler et al., 2016; Benali
108 et al., 2012; Zhang et al., 2011), and nighttime LST has an even higher correlation with T_{\max} than
109 daytime LST (Zeng et al., 2015; Zhang et al., 2011). Benali et al. (2012) hypothesized that the
110 presence of cloud cover may decrease daytime warming levels, resulting in incorrect modeling
111 and negative effects of cloud cover on estimation accuracies. Oyler et al. (2016) instead attributed
112 this to the large microscale variability differences between daytime and nighttime LST.

113 Due to the scarcity of detailed cloud observations available, few studies have focused on the
114 potentially important effects of clouds on estimations of T_{air} using remotely sensed LST. This
115 study explores the effects of clouds on T_{air} estimation using MODIS LST based on detailed
116 half-hourly ground measurements and the daily China Meteorological Administration (CMA)
117 station observations. For the TP, sufficiently detailed observations are extremely rare and related
118 studies have not been conducted before. Three automatic weather stations (AWS) with half-hourly
119 averaged observations are examined in this study, including one valuable site positioned on the
120 glacier. To make our study more representative, data drawn from 92 CMA stations that include
121 daily T_{\max} and T_{\min} observations are also used for cloud effect tests.

122 **2 Data**

123 **2.1 Ground measurements**

124 To conduct this study, detailed observations drawn from three AWSs on the TP were obtained (Fig.
125 1). The Ngari station is located in the western area of the TP at an elevation of 4270 m. Desert
126 grassland constitutes the main form of land cover here. The Qinghai station is located in the
127 northeastern TP at an elevation of 3250 m and is dominated by alpine meadow. The Xiao
128 Dongkemadi station is located in the interior TP at an elevation of 5621 m on the Xiao
129 Dongkemadi glacier (Fig. 1). The general features of the three AWSs are listed in Table 1. In
130 addition, observations drawn from 92 CMA stations over the TP are used for our assistant
131 analysis.

132 All three AWSs provide half-hourly averaged ingoing and outgoing longwave radiation, and air
133 temperature data. These radiation data were measured using a widely used CNR1 net radiometer,
134 at an uncertainty level of $\pm 10\%$ for daily totals by the manufacture. Air temperatures were
135 collected using an HMP45C sensor with expected accuracies of $\pm 0.2\text{--}0.5$ °C depending on the



136 temperature ranges involved. Detailed measurement specifications are listed in Table 1. However,
137 only the Xiao Dongkemadi station provides the directly measured LST values which were
138 obtained through an Apogee Precision Infrared Thermocouple Sensor (IRTS-P) with an accuracy
139 of 0.3 K over the glacier surface (Huitjes et al., 2015). The LSTs of the Qinghai and Ngari
140 stations were derived based on the thermal radiative transfer theory:

$$L_u = \sigma T_b^4 = (1 - \varepsilon)L_d + \varepsilon\sigma T_s^4$$

141 where L_u and L_d are the upwelling and downwelling longwave radiation, respectively, σ is the
142 Stefan–Boltzmann constant ($5.670367 \times 10^{-8} \text{ W m}^{-2} \text{ K}^{-4}$), ε is land surface emissivity, T_b is the
143 brightness temperature, T_s is the land surface temperature.

144 In this study, emissivity values were assigned empirically due to a lack of measurements.
145 Emissivity values for the Qinghai and Ngari stations were set to 0.987 (alpine meadow) and 0.975
146 (desert grassland), respectively, according to Wang et al. (2008). To partly quantify the effects of
147 emissivity value uncertainty, simple sensitivity tests were conducted. A 0.001 change in emissivity
148 is on average found to result in the LST change of 0.015 K and 0.020 K for stations Qinghai and
149 Ngari, respectively.

150 Through controlling the data quality did by the data provider, obvious outliers have been removed
151 for all three AWSs. In addition, the 92 CMA stations provide daily T_{\max} and T_{\min} observations
152 measured at 2 m above the ground surface. Data drawn from these CMA stations are for 2007 to
153 2010.

154

155 2.2 MODIS Land Surface Temperatures

156 Daily 1-km LST products of MODIS level 3 collection 5 are used in this study including the data
157 from the Terra (MOD11A1) and Aqua (MYD11A1) satellites. Both Terra and Aqua generate two
158 daily observations, including one for the daytime and one for nighttime. The two overpass times
159 for Aqua are approximately 1:30 and 13:30 local time. For Terra, these times are approximately
160 10:30 and 22:30. Accurate view times can be derived from the product. The MODIS LST used
161 here is retrieved using the generalized Split-window algorithm (Wan and Dozier, 1996).
162 Accuracies are reported to range within 1 K, but the uncertainties and errors of emissivity used in
163 the MODIS LST product can be significant, which produces major errors (Wan et al., 2002). Each
164 grid of the MODIS LST product includes a quality control (QC) flag that ranges from 0 to 3



165 indicating the average errors of <1 K, 1–2 K, 2–3 K and >3 K. Records with a QC flag of 3 were
166 omitted in this study.

167 The MODIS observations are instantaneous, whereas the ground measurements used are
168 half-hourly averaged. To make them comparable, the timing of ground observations recorded on
169 Beijing time was converted to local solar time. Then, half-hourly observations that are within 15
170 minutes of the view times of MODIS record times were selected.

171

172 **3 Methods**

173 **3.1 Cloud index estimations**

174 Cloud observations are usually only available from non-automatic weather stations and are
175 difficult to record. In this study, an efficient method was employed to estimate cloudiness based on
176 downwelling longwave radiation (L_d) records and air temperatures, which have been widely used
177 in other studies (Yang et al., 2011; Østby et al., 2014; Giesen et al., 2008). This theory is mainly
178 based on the principle that under cloudy conditions, a longwave radiation balance exists between
179 cloud base and near surface (Østby et al., 2014; Giesen et al., 2008). Under overcast conditions,
180 both the cloud base and near surface radiate at similar temperatures and L_d reaches its max.
181 However, L_d should be much lower under clear conditions than under overcast conditions under
182 the same temperature. In such a case, L_d reaches its minimum. Thus, a max L_d can be reversed
183 using the Stefan–Boltzmann law under a given air temperature, and the min L_d can be regressed
184 using the polynomial fit of the lower 5th percentile of the L_d observations for each specified
185 temperature interval (1 K here). When L_d is assumed to linearly increase from clear to overcast
186 conditions at a given temperature, then a “cloud index” (CI) indicating the cloudiness can be
187 achieved (CI = 0 and 1 for clear and overcast skies respectively). Rather than the visually
188 observed percentage of cloud cover in the sky, the CI used here represents the optical thickness of
189 clouds (Van Den Broeke et al., 2006).

190

191 **3.2 Testing cloud effects on the accuracies of MODIS LST**

192 Undetected clouds may exist in the MODIS LST data as a result of erroneous cloud identification.
193 An evaluation of the number of undetected clouds present was firstly conducted. As considerable
194 errors can be introduced by undetected clouds, the effects of clouds on MODIS LST accuracies



195 were evaluated by comparing validation (MODIS vs. observed LST) results derived before and
196 after removing the undetected cloudy records. In this study, the records with $CI > 0.5$ are
197 considered to be under “mostly cloudy” conditions. For a given MODIS observation, it is regarded
198 as undetected cloud if its corresponding $CI > 0.5$.

199 In our study, all four MODIS observations drawn from the Terra and Aqua satellites were
200 validated to identify and explain the effects of clouds on T_{air} estimations.

201

202 3.3 T_{air} estimation

203 A simple linear regression was used for T_{air} estimations. This method has been the most commonly
204 used in previous studies (Benali et al., 2012; Lin et al., 2012; Zhang et al., 2011). Although more
205 advanced models, including neural network (Jang et al., 2004), random forests (Xu et al., 2014)
206 and M5 model tree (Emamifar et al., 2013), can be more accurate, they can also introduce
207 uncertainties owing to their much larger number of parameters. Because an individual linear fit is
208 built for each AWS or CMA station, variables indicating spatial coordinates (longitudes and
209 latitudes) and land cover (e.g. NDVI) are not used. Thus, only LST is selected as the independent
210 variable for T_{air} regression. This is also why the machine learning methods and geostatistical
211 models (Oyler et al., 2015; Kilibarda et al., 2014) which generally involve the use of multiple
212 variables, are not used in this study.

213

214 3.4 Testing cloud effects by the observed LST

215 Large MODIS LST errors may exist due to undetected clouds, and cloud effects are first tested
216 using the ground measured LST. In this way, we can explore the direct effects of clouds on T_{air}
217 estimation using LST. The tests are conducted by constraining cloudiness conditions. Target T_{air}
218 values in most studies are daily (max, mean or min) values, but instantaneous cloudiness is
219 meaningless. In this study, the daily mean CI value is used as a cloudiness indicator. To ensure a
220 sufficient number of samples, 9 types of conditions with daily mean CI values $\leq 0.2, 0.3, \dots, 0.9$
221 and 1.0 are employed, indicating that the cloudiness constraints vary from highly clear conditions
222 (daily mean $CI \leq 0.2$) to fully mixed conditions, with many highly cloudy days included (daily
223 mean $CI \leq 1.0$). For each condition, T_{max} and T_{min} are regressed using daytime (13:30, Aqua) and
224 nighttime (22:30, Terra) observed LST through a simple linear regression, and estimation



225 accuracies are computed. The root-mean-square error (RMSE) and mean absolute error (MAE) are
226 used as the accuracy measurements. Cloud effects are evaluated based on the variation of the
227 estimation accuracies under different cloudiness conditions. Comparisons of T_{\max} and T_{\min}
228 estimations can reveal further implications of cloud effects.

229

230 **3.5 Determining cloud effects through comparisons using MODIS and the observed LST**

231 Once the effects of clouds on T_{air} estimations using observed LST are confirmed, cloud effects on
232 T_{air} estimation using MODIS LST can be explored more directly. Apart from affecting the
233 relationship between T_{air} and MODIS LST, clouds can degrade the MODIS LST accuracy and
234 further reduce estimation accuracies. Such effects, when they are present, can be explored by
235 comparing changes in estimation accuracy levels between observed LST and MODIS LST. Here,
236 T_{air} (T_{\min} and T_{\max}) estimations for 9 kinds of CI conditions are conducted using MODIS LST and
237 observed LST (at the corresponding MODIS time), respectively. The results are analyzed based on
238 comparisons.

239

240 **3.6 Exploring cloud effects based on observations from meteorological stations**

241 In practice, only daily observations can be easily obtained from meteorological stations, and
242 cloudiness observations are usually not provided. In this study, only daily T_{\max} and T_{\min} data are
243 obtained from the 92 CMA stations. Nonetheless, daily cloudiness levels can be partly evaluated
244 from four MODIS observations for each day (two from Terra and two from Aqua). Then,
245 comparisons of T_{air} estimation for two distinct cloudiness conditions are drawn.

246 Two conditions (“cloudy day” and “non-cloudy day”) are defined based on four instantaneous
247 MODIS observations for each day for both the T_{\max} and T_{\min} estimation using Aqua daytime LST
248 and Terra nighttime LST, respectively. For “non-cloudy day” conditions, all four MODIS
249 cloudiness observations are constrained as non-cloudy. For the “cloudy day” condition of the T_{\max}
250 estimation, Aqua daytime observations are constrained as non-cloudy to obtain the available LST,
251 and Terra daytime observations are constrained as cloudy to make cloud effects as strong as
252 possible. However, the Aqua night and Terra night observations are not constrained to obtain
253 sufficient samples. For the “cloudy day” condition of the T_{\min} estimation, the Terra nighttime
254 observations are constrained as non-cloudy to obtain the available LST, whereas the Aqua



255 nighttime observations are not constrained to obtain sufficient samples. Both Aqua daytime and
256 Terra daytime observations are constrained as cloudy to make the cloud effects as strong as
257 possible. T_{\max} and T_{\min} estimation accuracies are then compared under “cloudy day” and
258 “non-cloudy day” conditions.

259

260 **4 Result**

261 **4.1 Cloud index estimation and the undetected clouds of MODIS**

262 Figure 2 shows that the maximum and minimum L_d curves effectively frame L_d variation for each
263 air temperature. The CI values of all of the observations are then computed.

264 For each of the four overpass times of MODIS LST, a rate of undetected cloudy records can be
265 determined using CI values (Table 2). The ratio of undetected cloudy records ranges from 3% to
266 50% with a fully averaged ratio of 15%. This agrees well with the reported value of ~15%, which
267 was computed based on a consistency comparison between MODIS and Lidar (Ackerman et al.,
268 2008).

269

270 **4.2 MODIS LST validation under different cloud conditions**

271 The accuracy of MODIS LST can be affected by undetected cloudy pixels (Shamir and
272 Georgakakos, 2014; Westermann et al., 2012). Figure 3 shows that after removing cloudy cases,
273 the validation accuracies of all three sites present obviously lower MAE values and a better fit line
274 slope. Improvements in accuracy for 6 (2 pass times \times 3 stations) nighttime cases range from 0.1
275 to 0.9 °C. However, no significant accuracy improvements were found after removing cloudy
276 cases for daytime MODIS LST (Fig. 4). Only slightly better or comparative MAEs (≤ 0.1 °C)
277 were obtained.

278 This indicates that the accuracy of MODIS nighttime LST is more negatively affected by
279 undetected clouds than that for the daytime. The relatively weak influences of undetected clouds
280 on daytime LST is mainly due to obviously lower erroneous rates of cloud detection compared to
281 those of nighttime LST. Erroneous rates of MODIS nighttime cloud detection are clearly larger
282 than those for the daytime, though not in the case of the Terra LST observed for Ngari. This can be
283 largely attributed to differences in cloud detection methods used for the daytime and nighttime.
284 The cloud detection algorithm of MODIS is considered to present more confidence for the



285 daytime than for the nighttime due to the absence of reflected solar radiation during nighttime
286 (Ackerman et al., 1998). This finding is consistent with previous studies showing that more than
287 40% of the observed cloudy days are identified as clear days by MODIS at polar summer
288 nighttime (Østby et al., 2014).

289

290 **4.3 The effects of clouds on T_{air} estimation based on ground observed LST**

291 Figure 5 shows the accuracy of T_{air} estimations based on ground observed LST under different
292 cloudiness conditions across the three sites. For T_{max} , estimation errors including RMSE and MAE
293 continually increased as the cloudiness condition constraints eased. The increase in RMSE/MAE
294 values for clear conditions (daily mean CI ≤ 0.2) compared with totally mixed conditions (daily
295 mean CI ≤ 1) was 1.3 °C/1.0 °C, 0.8 °C/0.8 °C and 1.6 °C/1.6 °C for the Ngari, Xiao
296 Dongkemadi and Qinghai stations, respectively. In contrast, for T_{min} , accuracy variation is
297 consistently mild across the three sites, presenting RMSE/MAE changes of 0.1 °C/0.0 °C,
298 0.1 °C/0.0 °C, and 0.7 °C/0.6 °C for the Ngari, Xiao Dongkemadi and Qinghai stations,
299 respectively.

300 As expected for cases based on ground observed LST, the T_{max} estimation is significantly affected
301 by cloud conditions, but clouds have a limited effect on the T_{min} estimation compared to T_{max} . This
302 interesting finding can be explained by mechanisms through which clouds affect nighttime and
303 daytime surface temperatures. In the daytime, LST is significantly influenced by solar heating.
304 The presence of clouds can screen out solar radiation and cool the surface. Much larger
305 differences between LST and T_{air} have been observed under cloudy days than under clear
306 conditions (Gallo et al., 2011). At night, the surface can also present warming effects from clouds
307 due to reflected infrared longwave radiation. However, such effects are not typically significant
308 because the net effect of clouds on surface downward longwave radiation is much less pronounced
309 than nighttime solar cooling effects in most cases, as indicated by Dai et al. (1999).

310

311 **4.4 The effects of clouds on T_{air} estimation based on MODIS LST**

312 Figure 6 compares cloud effects on T_{min} and T_{max} estimations using MODIS and observed LST.
313 First, despite rather mild effects of cloud conditions on T_{min} estimation based on ground observed
314 LST, those based on MODIS LST are clearly much more significant. For cases based on MODIS



315 LST, increases in RMSE between clear (daily mean CI \leq 0.2) and mixed conditions (daily mean
316 CI \leq 1.0) are 0.5, 0.8, and 1.8 °C for the Ngari, Xiao Dongkemadi and Qinghai stations,
317 respectively. However, those for cases based on observed LST are significantly lower with
318 corresponding values of 0.0, -0.1, and 0.2 °C.

319 This indicates that T_{\min} estimations based on MODIS LST are greatly affected by clouds. This
320 seems counterintuitive, as it has been shown that T_{\min} estimations based on ground observed LST
321 are not significantly affected by clouds (Fig. 5). Thus, the most probable driving factor may be the
322 relatively large amounts of undetected clouds present in MODIS nighttime LST. As daily cloud
323 indexes increase, more undetected cloudy cases may be introduced, thus reducing the accuracy of
324 MODIS nighttime LST (Fig. 3 and Table 2).

325 Figure 7 (upper section) supports this conclusion: under clear conditions, the undetected clouds
326 are rare, and limited accuracy improvements are achieved by removing the few cloudy MODIS
327 LST records; However, as daily CI constraints ease to 0.5 when cloudy records account for a
328 substantial proportion, obvious improvements appear, and the final accuracies are much closer to
329 and are even better than those based on ground observed LST.

330 Unlike that of T_{\min} , the accuracy variation of T_{\max} estimation based on MODIS LST shows trends
331 that are highly consistent with those of cases based on ground observed LST for all of the three
332 sites. As with cases based on ground observed LST, T_{\max} estimation based on MODIS LST are
333 found to be greatly affected by clouds. In addition, increases in (T_{\max} estimation based on MODIS
334 LST vs. that based on ground observed LST) in accuracy level differences between clear and
335 mixed conditions are much less pronounced compared to those of T_{\min} , where difference values
336 are only 0.0, 0.2 and 0.3 °C for the Ngari, Xiao Dongkemadi and Qinghai stations, respectively.

337 However, the accuracy levels achieved from MODS LST after removing cloudy records are
338 obviously lower than those based on ground observed LST under all cloudiness conditions. This
339 raises questions regarding what this difference in accuracy attribute to? Dominant factors may not
340 be undetected clouds, as was the case for T_{\min} . As shown in Fig. 7 (lower section), the removal of
341 cloudy records had somewhat moderate effects on accuracy levels. This may be largely due to
342 much lower erroneous rates of cloud identification for MODIS daytime LST. The obviously lower
343 number of undetected clouds compared to nighttime LST values for the Ngari and Qinghai
344 stations result in relatively limited accuracy improvements. The relatively large decrease in



345 estimation errors for the Xiao Dongkemadi station is mainly due to unexpected higher amounts of
346 undetected clouds in MODIS daytime LST for that site (Table 2 and Fig. 7).

347 Furthermore, even under clear conditions, the accuracy of T_{\max} estimations based on MODIS LST
348 is remarkably lower than that based on ground observed LST (Fig. 6). Thus, the decrease in
349 accuracy levels relative to cases based on ground observed LST may be caused by other factors
350 rather than undetected clouds. This seems odd, especially given that the accuracies of T_{\min}
351 estimations based on MODIS LST are very close to or even better than those based on observed
352 LST under clear conditions (Fig. 6).

353

354 **4.5 Effects of clouds on T_{air} estimation based on MODIS LST and CMA observations**

355 Figure 8 shows the estimation accuracies of T_{air} based on MODIS LST for non-cloudy and cloudy
356 conditions. For the T_{\max} estimation, clouds appear to have moderate effects on estimation
357 accuracies, where 88% of the 92 stations obtained lower RMSEs based on samples from
358 “non-cloudy” conditions relative to cloudy cases. RMSE values are reduced by an average of
359 0.54 °C. In contrast, effects of clouds on T_{\min} estimations are much more significant: the RMSEs
360 of 98% stations are reduced by an average of 1.44 °C. Though hourly observations in the data for
361 CMA stations are lacking, the results for the cloud tests are highly consistent with those based on
362 half-hourly AWS observations.

363 Furthermore, a comparison between the T_{\max} and T_{\min} estimation results based on MODIS LST
364 and CMA observations shows that under cloudy conditions, T_{\max} estimations (the mean RMSE is
365 4.3 °C) achieve generally higher levels of accuracy than T_{\min} estimations (the mean RMSE is
366 4.6 °C), whereas non-cloudy conditions produce the opposite effect (3.7 vs. 3.2 °C) illustrating
367 potentially stronger negative effect of cloud on T_{\max} estimation than T_{\min} .

368

369 **5 Discussion**

370 **5.1 Differences in the effects of clouds on T_{\min} and T_{\max} estimations based on MODIS LST**

371 From MODIS LST and daily CMA observations, different cloud effects between T_{\max} and T_{\min}
372 estimations can be identified from Fig. 8. Under cloudy conditions, the existence of more
373 undetected cloudy records in MODIS nighttime LST largely degrades the LST accuracy and
374 results in obviously lower T_{\min} estimation accuracy levels. However, why the T_{\min} estimations



375 clearly outperform T_{\max} under clear conditions (non-cloudy day condition) when both are free of
376 cloud effects remains unknown. One may argue that the so-called “clear” conditions are based on
377 only four satellite instantaneous observations and that actual cloudiness conditions may still be
378 cloudy. Although this is true, our study shows that even under clear conditions, the accuracy of
379 T_{\max} estimations based on daytime MODIS LST is much lower than those based on observed LST,
380 whereas the T_{\min} estimation based on nighttime MODIS LST shows comparable or even superior
381 accuracy.

382 From our previous analysis, we can attribute this difference in estimation accuracy between T_{\min}
383 and T_{\max} to differences between daytime and nighttime MODIS LST. Much lower levels of
384 MODIS daytime LST accuracy than those for nighttime have been found in previous studies
385 (Krishnan et al., 2015; Min et al., 2015; Yu and Ma, 2011), and the validation tests shown in Sect.
386 4.2 also supports this conclusions. This precision bias is most likely attributable scale issues (Wan
387 et al., 2002; Wan, 2008). Single point measurements are difficult to make representative of the
388 1-km MODIS pixel when ground surfaces are complex (Coll et al., 2009; Hall et al., 2008). Many
389 studies have shown that MODIS daytime LST presents obviously lower levels of validation
390 accuracy than nighttime LST due to high levels of daytime LST heterogeneity (Wang et al.,
391 2008; Coll et al., 2009). In the daytime, cloud and hill shadows within pixels can produce
392 considerable LST heterogeneities while at night, the ground surface becomes cool and more
393 homogeneous when free of solar heating uncertainties (Wang et al., 2008). Oyler et al. (2016) also
394 show that daytime LST exhibits more spatial variation than T_{air} while nighttime LST follows
395 similar spatial patterns as T_{air} as demonstrated in his study.

396 In addition, it should be noted that clouds also have substantial effects on T_{\max} estimation. Thus, it
397 can be concluded that the frequently reported lower estimation accuracies of T_{\max} based on
398 MODIS daytime LST compared to those of T_{\min} based on nighttime LST (Zhu et al., 2013; Benali
399 et al., 2012; Zhang et al., 2011; Oyler et al., 2016) are mainly due to the mixed effects of \the
400 relatively low daytime LST accuracies and clouds.

401 To further prove this, four CMA stations (Fig. 9) presenting the largest reduction in RMSE values
402 after imposing clear conditions are selected for our T_{\min} and T_{\max} estimations. They can represent
403 practical application conditions where only daily meteorological observations can be obtained.

404 For T_{\max} estimation (Fig. 10), it is evident that forcing clear conditions has somewhat limited



405 effects on estimation performance. The samples collected under “cloudy day” conditions include
406 outliers far from the fit line derived using samples under “non-cloudy day” conditions. However,
407 the “non-cloudy day” samples still appear rather dispersed with many samples positioned far from
408 the fit line, and especially in the case of stations 89 and 41. This may illustrate mixed effects of
409 both clouds and LST accuracies to some degree.

410 In contrast, the results of the T_{\min} estimation are somewhat inspiring. As shown in Fig. 11, a
411 number of cold-biased outliers that may be undetected cloudy records are captured by employing
412 cloudy conditions. More importantly, the “non-cloudy day” condition samples achieve a much
413 better fit. This not only demonstrates that undetected cloudy records are ubiquitous in MODIS
414 nighttime LST and that amounts can often be quite large but also that the influence of clouds on
415 T_{\min} estimations with true LST (i.e., without undetected clouds) is not substantial. Though the
416 actual cloudiness conditions are rather unpredictable and quite a few “good” samples around the
417 “non-cloudy day” fit line are also included in the “cloudy day” group, we consider constraining all
418 four MODIS observations for each day as non-cloudy as an efficient way to build a good fit
419 among T_{\min} estimations using MODIS nighttime LST as long as the amount of valid samples is
420 sufficient. This method can benefit studies requiring accurate T_{\min} estimations based on remotely
421 sensed LST.

422

423 5.2 Uncertainty and error sources

424 Emissivity issues may have caused the observed LST computation errors. Constant emissivity
425 values for the Ngari and Qinghai stations are used in our study, although this may not be
426 reasonable for non-growing seasons. However, the sensitivity experiments show that the influence
427 of emissivity values is not significant.

428 The ≤ 15 min discrepancy may introduce uncertainties in data that intersect T_{air} , MODIS and
429 observed LST. Its influence is considered to be insignificant. Nighttime LST changes gently and
430 half-hourly observations can be used for MODIS LST validation as indicated in Wang et al.
431 (2008). T_{air} also respond relatively slowly to LST, and MODIS daytime LST shows a strong
432 relationship to T_{air} at a similar time discrepancy level (≤ 12 min) to that shown by Williamson et al.
433 (2013). Spatial heterogeneities within MODIS pixels of AWS may pose problems. As shown in
434 Fig. 1, such problems may not be severe, as land cover within the pixels of the three AWSs



435 appears to be largely homogeneous. The data quality of MODIS LST does not receive sufficient
436 consideration in this study. MODIS LST production involves the use of internal data quality flags,
437 and previous studies demonstrate that data quality is related to cloud contamination (Williamson et
438 al., 2013; Østby et al., 2014).

439 The validation accuracy of MODIS LST is affected by data quality (Krishnan et al., 2015).
440 However, rigid data quality constraints may severely decrease sample sizes due to relatively short
441 observation periods (1–2 years) used. This study presents results of general quality status, and
442 extreme low quality data (QC = 3) have been removed. Other factors including wind speeds and
443 sensor view zenith angles may affect results related to MODIS LST validation and the relationship
444 between T_{air} and LST. According to Wang et al. (2008), the validation results are not or are weakly
445 affected by wind speed and the sensor view zenith angle. Wind speed has a limited effect on the
446 T_{air} -LST relationship, as shown by Gallo et al. (2011).

447 In addition, the results shown here are highly consistent across the three AWSs dominated by three
448 types of land cover, thus indicating that our results may be highly representative and that other
449 factors may not have played a key role in this study.

450

451 **6 Conclusion**

452 Cloud effects on T_{min} and T_{max} estimations according to MODIS LST are analyzed based on
453 detailed ground based observations drawn from three valuable AWSs and based on data drawn
454 from 92 CMA stations over the TP. Cloudiness is quantified using an efficient method based on
455 ground measurements of air temperature and downwelling longwave radiation. Comparisons made
456 between in-situ cloudiness observations and MODIS claimed clear-sky records shows that
457 erroneous rates of MODIS nighttime cloud detection are obviously larger than those for the
458 daytime. Our MODIS LST validation for different cloudiness constraining conditions reveals that
459 the accuracy of MODIS nighttime LST is severely affected by undetected clouds. However, the
460 accuracies of MODIS daytime LST do not seem to be influenced considerably by undetected
461 clouds.

462 Cloud effect tests show that T_{min} estimations based on MODIS LST are mainly affected by large
463 errors introduced by undetected clouds in nighttime LST. However, clouds mainly influence T_{max}
464 estimation by affecting the relationship between T_{max} and daytime LST. The effects of undetected



465 clouds in daytime LST are relatively weak. Frequently reported larger errors in T_{\max} estimations
466 based on daytime LST than those of T_{\min} based on nighttime LST may be largely attributed to
467 relatively large errors of MODIS daytime LST resulting from scale issues. Tests based on CMA
468 station observations further validate our results and show that constraining all four MODIS
469 observations per day as non-cloudy helps rule out undetected cloudy records while building good
470 T_{\min} estimation fit.

471 This study presents useful findings on the key effects of clouds on T_{air} estimation based on
472 MODIS LST that can alleviate problems of severe data sparseness over the TP. More efficient
473 cloud detection methods for MODIS nighttime LST are needed for T_{\min} estimations. T_{\max}
474 estimation based on daytime LST is rather challenging due to the complex effects of daily
475 cloudiness conditions in combination with scale issues.

476

477 **Author Contribution**

478 Professor Tian, He and Tang observed and provided the data of stations Nagri, Xiao Dongkemadi
479 and Qinghai, respectively. Professor Fan Zhang and Associate Professor Guoqing Zhang gave
480 many valuable suggestions to improve the manuscript. Hongbo designed the experiments and
481 wrote the manuscript.

482

483 **Acknowledgment**

484 This work was supported by the Chinese Academy of Sciences “Strategic Priority Research
485 Program (B)” (Grant No. XDB03030300); and by the National Natural Science Foundation of
486 China (Grant No. 41422101, 41271079, 41130638). We thank the Tanggula Station for Cryosphere
487 Environment Observation and Research and the Ngari Station for Desert Environment
488 Observation and Research for providing ground measurements of longwave radiation and air
489 temperature data. The Qinghai station data were downloaded from AsiaFlux (www.asiaflux.net).
490 We would like to thank Dr. Yanhong Tang for providing the ground measurements for the Qinghai
491 station. We are grateful to the Chinese Meteorology Administration for providing air temperature
492 data.

493

494

495 **References**

- 496 Ackerman, S. A., Strabala, K. I., Menzel, W. P., Frey, R. A., Moeller, C. C., and Gumley, L. E.:
497 Discriminating clear sky from clouds with MODIS, *J. Geophys. Res.-Atmos.*, 103, 32141-32157,
498 10.1029/1998jd200032, 1998.
- 499 Ackerman, S. A., Holz, R. E., Frey, R., Eloranta, E. W., Maddux, B. C., and McGill, M.: Cloud Detection
500 with MODIS. Part II: Validation, *Journal of Atmospheric and Oceanic Technology*, 25, 1073-1086,
501 doi:10.1175/2007JTECHA1053.1, 2008.
- 502 Benali, A., Carvalho, A. C., Nunes, J. P., Carvalhais, N., and Santos, A.: Estimating air surface
503 temperature in Portugal using MODIS LST data, *Remote Sensing of Environment*, 124, 108-121,
504 <http://dx.doi.org/10.1016/j.rse.2012.04.024>, 2012.
- 505 Coll, C., Wan, Z., and Galve, J. M.: Temperature - based and radiance - based validations of the V5
506 MODIS land surface temperature product, *Journal of Geophysical Research: Atmospheres*, 114,
507 2009.
- 508 Dai, A., Trenberth, K. E., and Karl, T. R.: Effects of clouds, soil moisture, precipitation, and water vapor
509 on diurnal temperature range, *Journal of Climate*, 12, 2451-2473,
510 10.1175/1520-0442(1999)012<2451:eocsm>2.0.co;2, 1999.
- 511 Emamifar, S., Rahimkhoob, A., and Noroozi, A. A.: Daily mean air temperature estimation from MODIS
512 land surface temperature products based on M5 model tree, *International Journal of Climatology*,
513 33, 3174-3181, 10.1002/joc.3655, 2013.
- 514 Fu, G., Shen, Z., Zhang, X., Shi, P., Zhang, Y., and Wu, J.: Estimating air temperature of an alpine
515 meadow on the Northern Tibetan Plateau using MODIS land surface temperature, *Acta Ecologica*
516 *Sinica*, 31, 8-13, <http://dx.doi.org/10.1016/j.chnaes.2010.11.002>, 2011.
- 517 Gallo, K., Hale, R., Tarpley, D., and Yu, Y.: Evaluation of the relationship between air and land surface
518 temperature under clear-and cloudy-sky conditions, *Journal of Applied Meteorology and*
519 *Climatology*, 50, 767-775, 2011.
- 520 Giesen, R., Van den Broeke, M., Oerlemans, J., and Andreassen, L.: Surface energy balance in the
521 ablation zone of Midtdalsbreen, a glacier in southern Norway: interannual variability and the
522 effect of clouds, *Journal of Geophysical Research: Atmospheres*, 113, 2008.
- 523 Good, E.: Daily minimum and maximum surface air temperatures from geostationary satellite data,
524 *Journal of Geophysical Research: Atmospheres*, 120, 2306-2324, 10.1002/2014JD022438, 2015.
- 525 Hall, D. K., Box, J. E., Casey, K. A., Hook, S. J., Shuman, C. A., and Steffen, K.: Comparison of
526 satellite-derived and in-situ observations of ice and snow surface temperatures over Greenland,
527 *Remote Sensing of Environment*, 112, 3739-3749, 2008.
- 528 Huintjes, E., Sauter, T., Schröter, B., Maussion, F., Yang, W., Kropáček, J., Buchroithner, M., Scherer, D.,
529 Kang, S., and Schneider, C.: Evaluation of a coupled snow and energy balance model for Zhadang
530 glacier, Tibetan Plateau, using glaciological measurements and time-lapse photography, *Arctic*,
531 *Antarctic, and Alpine Research*, 47, 573-590, 2015.
- 532 Jang, J.-D., Viau, A., and Ancil, F.: Neural network estimation of air temperatures from AVHRR data,
533 *International Journal of Remote Sensing*, 25, 4541-4554, 2004.
- 534 Kilibarda, M., Hengl, T., Heuvelink, G. B. M., Gräler, B., Pebesma, E., Perčec Tadić, M., and Bajat, B.:
535 Spatio-temporal interpolation of daily temperatures for global land areas at 1 km resolution,
536 *Journal of Geophysical Research: Atmospheres*, 119, 2294-2313, 10.1002/2013JD020803, 2014.
- 537 Krishnan, P., Kochendorfer, J., Dumas, E. J., Guillevic, P. C., Baker, C. B., Meyers, T. P., and Martos, B.:
538 Comparison of in-situ, aircraft, and satellite land surface temperature measurements over a



- 539 NOAA Climate Reference Network site, *Remote Sensing of Environment*, 165, 249-264, 2015.
- 540 Langer, M., Westermann, S., and Boike, J.: Spatial and temporal variations of summer surface
541 temperatures of wet polygonal tundra in Siberia - implications for MODIS LST based permafrost
542 monitoring, *Remote Sensing of Environment*, 114, 2059-2069,
543 <http://dx.doi.org/10.1016/j.rse.2010.04.012>, 2010.
- 544 Lin, S. P., Moore, N. J., Messina, J. P., DeVisser, M. H., and Wu, J. P.: Evaluation of estimating daily
545 maximum and minimum air temperature with MODIS data in east Africa, *Int. J. Appl. Earth Obs.*
546 *Geoinf.*, 18, 128-140, 10.1016/j.jag.2012.01.004, 2012.
- 547 Lin, X., Pielke Sr, R. A., Mahmood, R., Fiebrich, C. A., and Aiken, R.: Observational evidence of
548 temperature trends at two levels in the surface layer, *Atmos. Chem. Phys.*, 16, 827-841,
549 10.5194/acp-16-827-2016, 2016.
- 550 Min, W., Yueqing, L. I., and Zhou, J.: Validation of MODIS Land Surface Temperature Products in East of
551 the Qinghai-Xizang Plateau, *Plateau Meteorology*, 2015.
- 552 Østby, T. I., Schuler, T. V., and Westermann, S.: Severe cloud contamination of MODIS Land Surface
553 Temperatures over an Arctic ice cap, Svalbard, *Remote Sensing of Environment*, 142, 95-102,
554 <http://dx.doi.org/10.1016/j.rse.2013.11.005>, 2014.
- 555 Oyler, J. W., Ballantyne, A., Jencso, K., Sweet, M., and Running, S. W.: Creating a topoclimatic daily air
556 temperature dataset for the conterminous United States using homogenized station data and
557 remotely sensed land skin temperature, *International Journal of Climatology*, 35, 2258-2279,
558 2015.
- 559 Oyler, J. W., Dobrowski, S. Z., Holden, Z. A., and Running, S. W.: Remotely Sensed Land Skin
560 Temperature as a Spatial Predictor of Air Temperature across the Conterminous United States,
561 *Journal of Applied Meteorology and Climatology*, 2016.
- 562 Parmentier, B., McGill, B. J., Wilson, A. M., Regetz, J., Jetz, W., Guralnick, R., Tuanmu, M. N., and
563 Schildhauer, M.: Using multi - timescale methods and satellite - derived land surface
564 temperature for the interpolation of daily maximum air temperature in Oregon, *International*
565 *Journal of Climatology*, 35, 3862-3878, 2015.
- 566 Shamir, E., and Georgakakos, K. P.: MODIS Land Surface Temperature as an index of surface air
567 temperature for operational snowpack estimation, *Remote Sensing of Environment*, 152, 83-98,
568 2014.
- 569 Shen, S. H., and Leptoukh, G. G.: Estimation of surface air temperature over central and eastern
570 Eurasia from MODIS land surface temperature, *Environ. Res. Lett.*, 6, 8,
571 10.1088/1748-9326/6/4/045206, 2011.
- 572 Van Den Broeke, M., Reijmer, C., Van As, D., and Boot, W.: Daily cycle of the surface energy balance in
573 Antarctica and the influence of clouds, *International Journal of Climatology*, 26, 1587-1605,
574 10.1002/joc.1323, 2006.
- 575 Vancutsem, C., Ceccato, P., Dinku, T., and Connor, S. J.: Evaluation of MODIS land surface temperature
576 data to estimate air temperature in different ecosystems over Africa, *Remote Sensing of*
577 *Environment*, 114, 449-465, <http://dx.doi.org/10.1016/j.rse.2009.10.002>, 2010.
- 578 Wan, Z., and Dozier, J.: A generalized split-window algorithm for retrieving land-surface temperature
579 from space, *Geoscience and Remote Sensing, IEEE Transactions on*, 34, 892-905, 1996.
- 580 Wan, Z., Zhang, Y., Zhang, Q., and Li, Z.-l.: Validation of the land-surface temperature products
581 retrieved from Terra Moderate Resolution Imaging Spectroradiometer data, *Remote sensing of*
582 *Environment*, 83, 163-180, 2002.



- 583 Wan, Z.: New refinements and validation of the MODIS Land-Surface Temperature/Emissivity products,
584 Remote Sensing of Environment, 112, 59-74, <http://dx.doi.org/10.1016/j.rse.2006.06.026>, 2008.
- 585 Wang, W., Liang, S., and Meyers, T.: Validating MODIS land surface temperature products using
586 long-term nighttime ground measurements, Remote Sensing of Environment, 112, 623-635,
587 2008.
- 588 Westermann, S., Langer, M., and Boike, J.: Spatial and temporal variations of summer surface
589 temperatures of high-arctic tundra on Svalbard - Implications for MODIS LST based permafrost
590 monitoring, Remote Sensing of Environment, 115, 908-922, 10.1016/j.rse.2010.11.018, 2011.
- 591 Westermann, S., Langer, M., and Boike, J.: Systematic bias of average winter-time land surface
592 temperatures inferred from MODIS at a site on Svalbard, Norway, Remote Sensing of
593 Environment, 118, 162-167, 2012.
- 594 Williamson, S. N., Hik, D. S., Gamon, J. A., Kavanaugh, J. L., and Koh, S.: Evaluating cloud contamination
595 in clear-sky MODIS Terra daytime land surface temperatures using ground-based meteorology
596 station observations, Journal of Climate, 26, 1551-1560, 2013.
- 597 Wu, Y., Wang, N., He, J., and Jiang, X.: Estimating mountain glacier surface temperatures from
598 Landsat-ETM+ thermal infrared data: A case study of Qiyi glacier, China, Remote Sensing of
599 Environment, 163, 286-295, 2015.
- 600 Xu, Y., Knudby, A., and Ho, H. C.: Estimating daily maximum air temperature from MODIS in British
601 Columbia, Canada, International Journal of Remote Sensing, 35, 8108-8121,
602 10.1080/01431161.2014.978957, 2014.
- 603 Yang, W., Guo, X., Yao, T., Yang, K., Zhao, L., Li, S., and Zhu, M.: Summertime surface energy budget and
604 ablation modeling in the ablation zone of a maritime Tibetan glacier, Journal of Geophysical
605 Research: Atmospheres, 116, 2011.
- 606 Yu, J., Zhang, G., Yao, T., Xie, H., Zhang, H., Ke, C., and Yao, R.: Developing Daily Cloud-Free Snow
607 Composite Products From MODIS Terra-Aqua and IMS for the Tibetan Plateau.
- 608 Yu, W., and Ma, M.: Validation of the MODIS Land Surface Temperature Products—A Case Study of
609 the Heihe River Basin, Remote Sensing Technology & Application, 26, 705-712, 2011.
- 610 Zeng, L., Wardlow, B. D., Tadesse, T., Shan, J., Hayes, M. J., Li, D., and Xiang, D.: Estimation of daily air
611 temperature based on MODIS land surface temperature products over the corn belt in the US,
612 Remote Sens., 7, 951-970, 2015.
- 613 Zhang, W., Huang, Y., Yu, Y. Q., and Sun, W. J.: Empirical models for estimating daily maximum,
614 minimum and mean air temperatures with MODIS land surface temperatures, International
615 Journal of Remote Sensing, 32, 9415-9440, 10.1080/01431161.2011.560622, 2011.
- 616 Zhu, W., Lú, A., and Jia, S.: Estimation of daily maximum and minimum air temperature using MODIS
617 land surface temperature products, Remote Sensing of Environment, 130, 62-73,
618 <http://dx.doi.org/10.1016/j.rse.2012.10.034>, 2013.
- 619
- 620
- 621



622 Table 1. Summary of the AWS sites

623

AWS	Lon/Lat	Mean annual Precipitation (mm)	Mean annual air temperature (°C)	Elevation (m)	Land cover	Time period
Xiao Dongkemadi	92.08/33.07	680	-8.6	5621	Glacier	2009.1 - 2009.12
Ngari	79.70/33.39	125	1.2	4270	Desert grassland	2012.6 - 2013.12
Qinghai	101.30/37.60	567	-1.7	3250	Alpine meadow	2003.1 - 2004.12

624



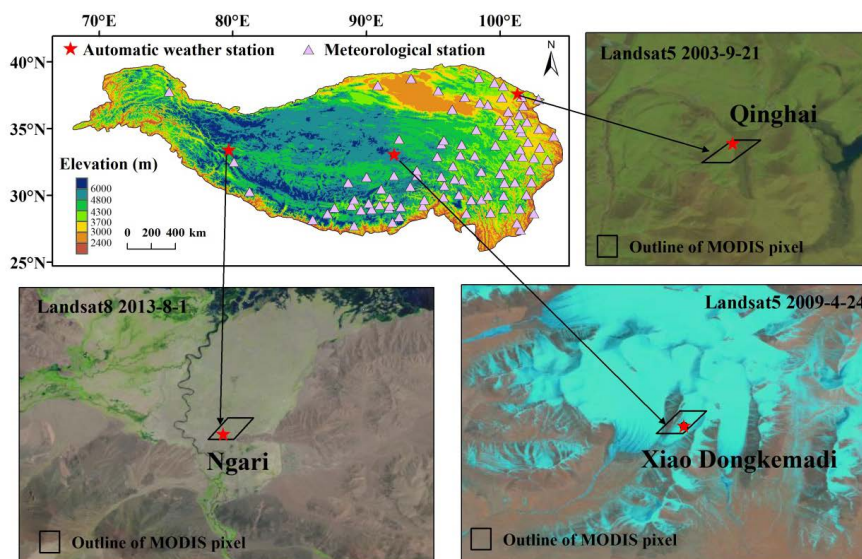
625 Table 2. Undetected MODIS LST clouds at 3 AWSs

626

Site	Ratio of undetected cloudy records			
	Terra day (%)	Terra night (%)	Aqua day (%)	Aqua night (%)
Ngari	5	3	3	15
Xiao Dongkemadi	12	15	11	37
Qinghai	3	20	3	50
Average	7	13	6	34

627

628



629

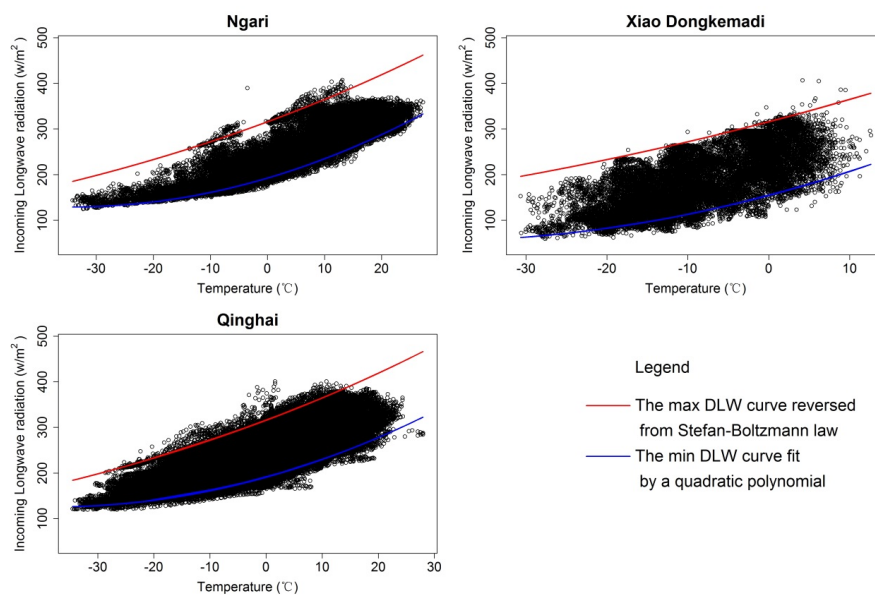
630

631 Figure 1: Map of the TP marking AWS and meteorological station locations. Landsat images
632 observed during the time period for data used in this study are also shown in natural color modes
633 with capturing dates. The outline of the MODIS grid is also plotted.

634



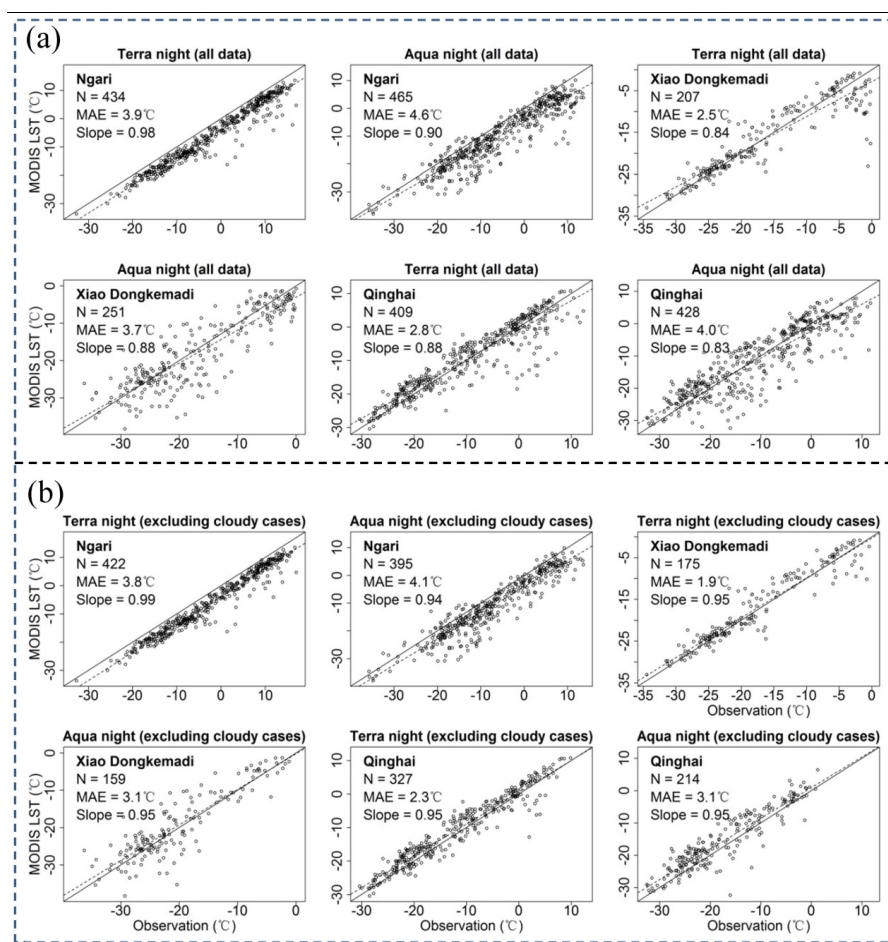
635



636

637 Figure 2: The distribution of downward longwave radiation (DLW) under different air
638 temperatures. The red line represents the max DLW curve reversed from the Stefan-Boltzmann
639 law. The blue line is the min DLW curve fitted by a quadratic polynomial.

640



641

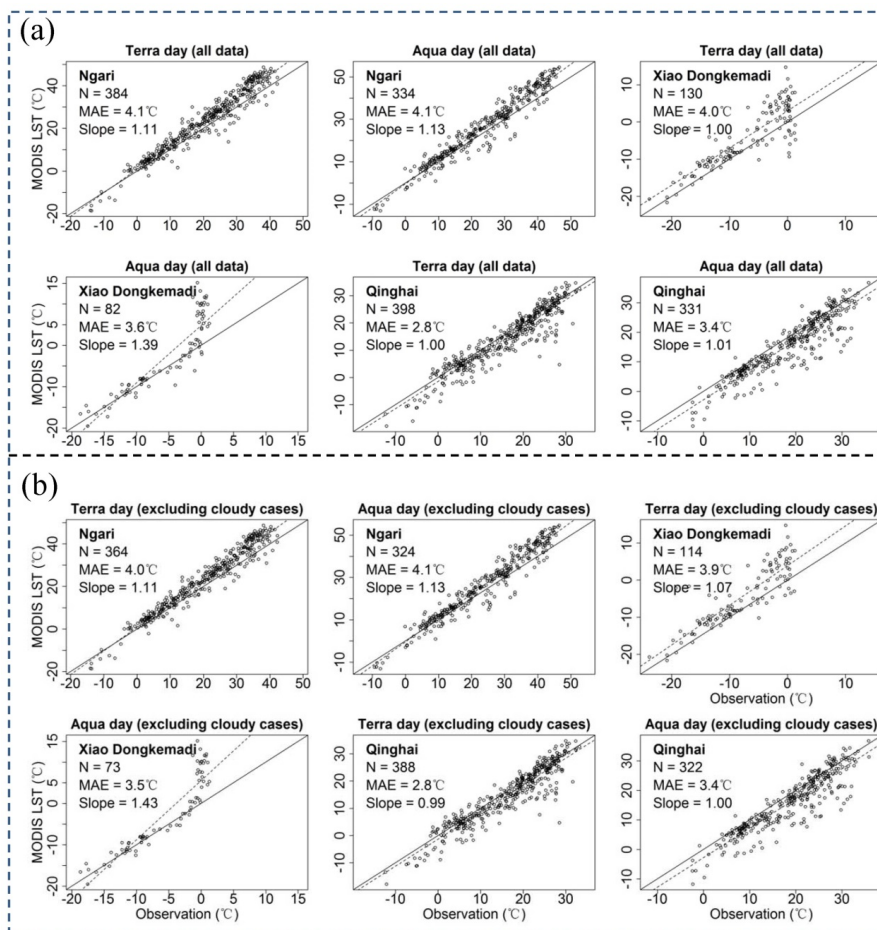
642

643 Figure 3: Validation of MODIS nighttime LST before (a) and after (b), excluding cloudy

644 cases.

645

646



647

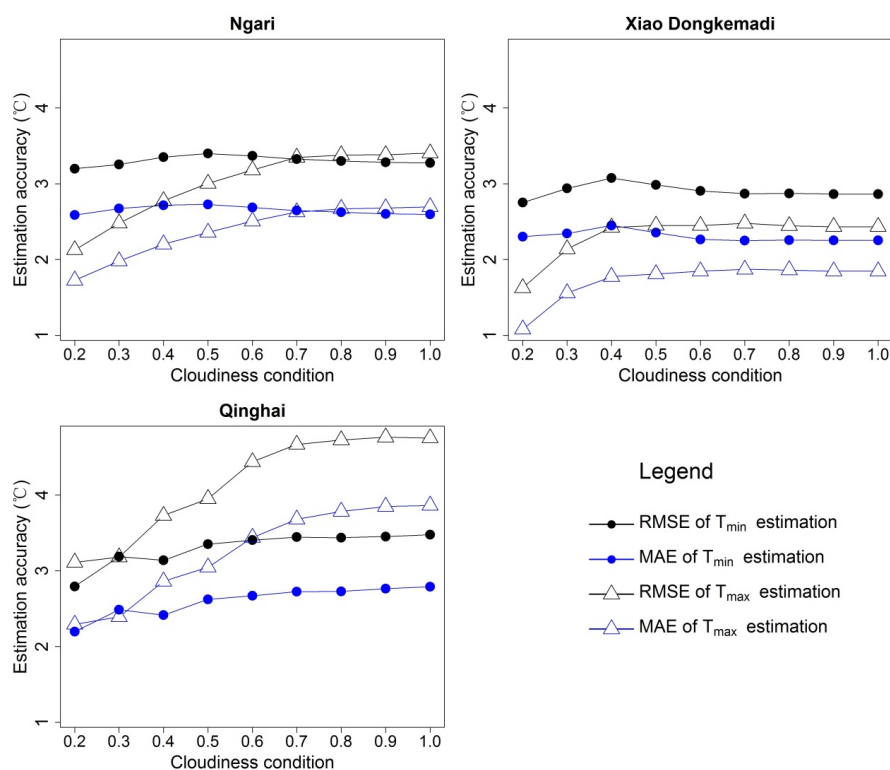
648

649 Figure 4: Validation of MODIS daytime LST before (a) and after (b), excluding cloudy cases.

650



651



652

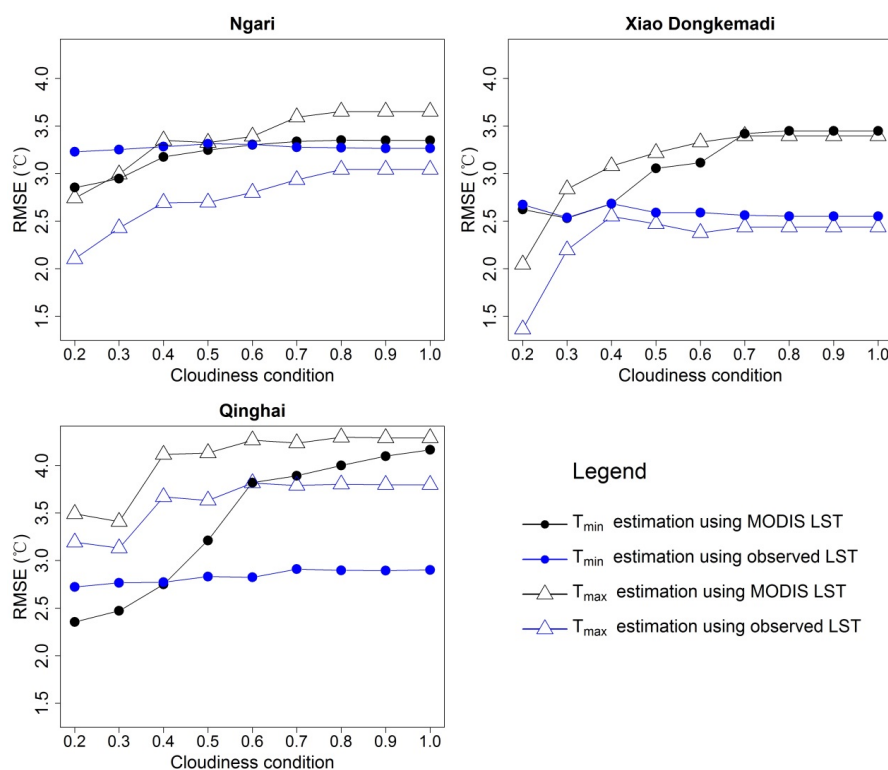
653

654 Figure 5: Accuracies (RMSE and MAE) of T_{max} and T_{min} estimations based on ground measured
 655 LST under different cloudiness conditions across the three sites. The “cloudiness condition” is the
 656 constraining condition of the daily averaged cloudiness index (CI). For example, a cloudiness
 657 condition of 0.2 denotes a constraining daily mean of $CI \leq 0.2$.

658



659



660

661

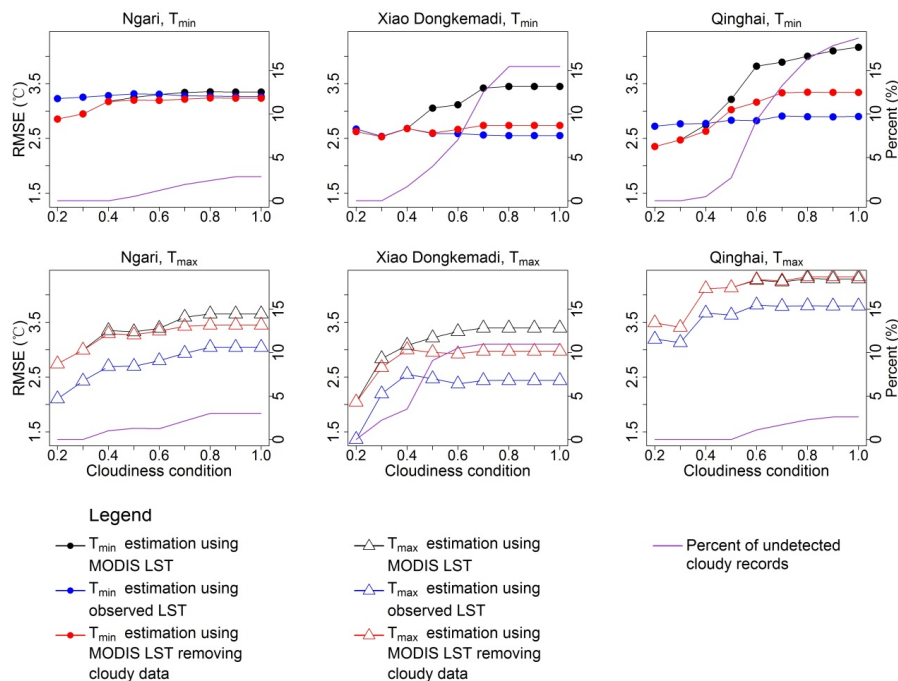
662 Figure 6: Accuracies (RMSE) of T_{max} and T_{min} estimations based on ground measured or MODIS

663 LST under different cloudiness conditions for the three AWSs. The “cloudiness condition” is the

664 constraining condition of the daily averaged cloudiness index (CI). For example, a cloudiness

665 condition of 0.2 denotes a constraining daily mean of $CI \leq 0.2$.

666



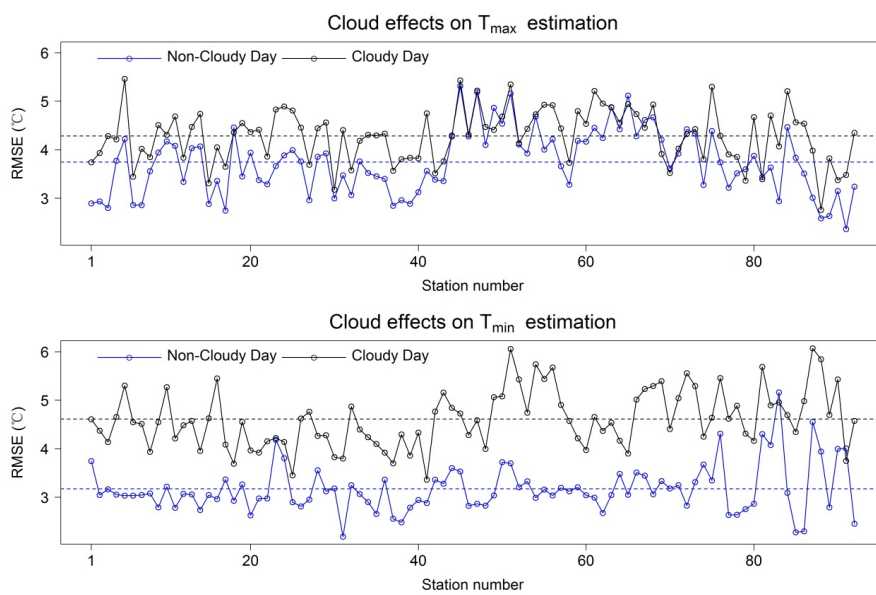
667

668 Figure 7: Comparisons between T_{min} and T_{max} estimation accuracies based on MODIS LST,

669 MODIS LST without cloudy data, and observed LST under different cloudiness conditions for the

670 three AWSs.

671



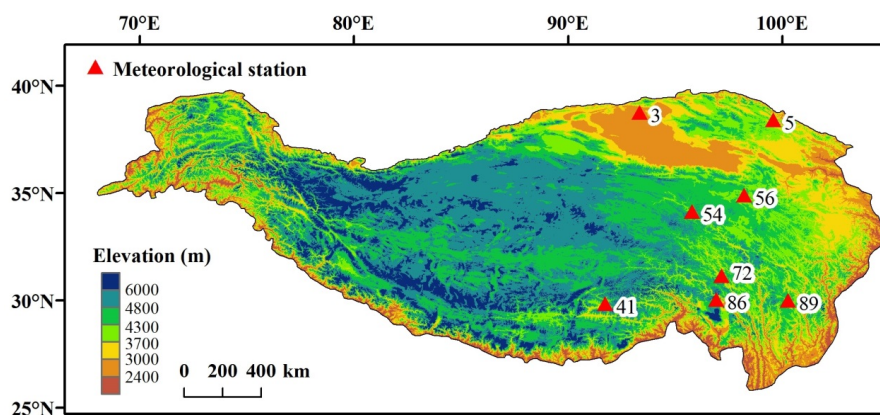
672

673

674 Figure 8: Comparisons of T_{air} estimation accuracy levels based on MODIS LST and CMA

675 observations for “non-cloudy day” and “cloudy day” conditions.

676



677

678

679 Figure 9: Locations of 4 representative CMA stations for T_{\min} (NO. 54, 56, 72, 86) and T_{\max} (NO.

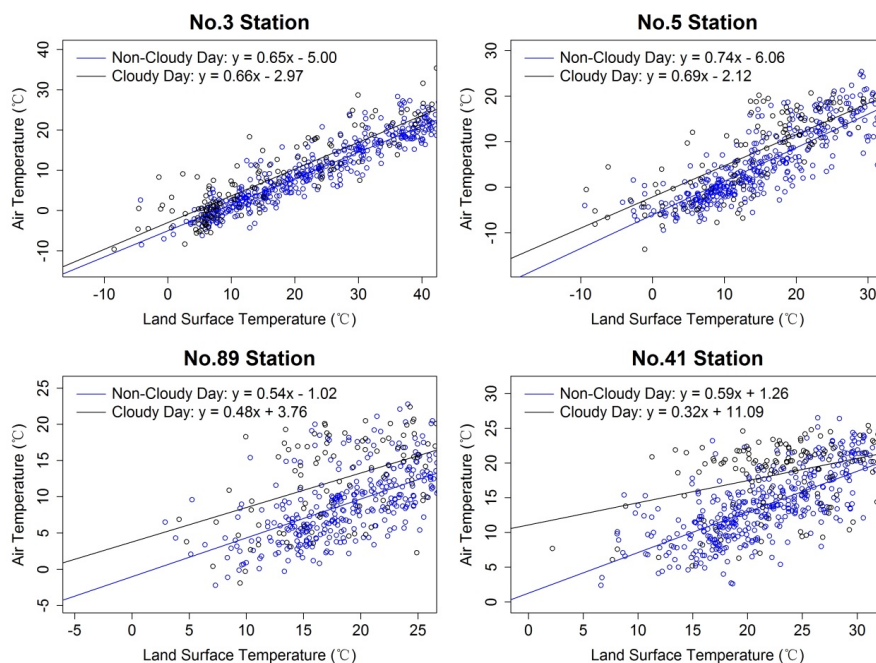
680 3, 5, 41, 89) estimations.

681



682

683



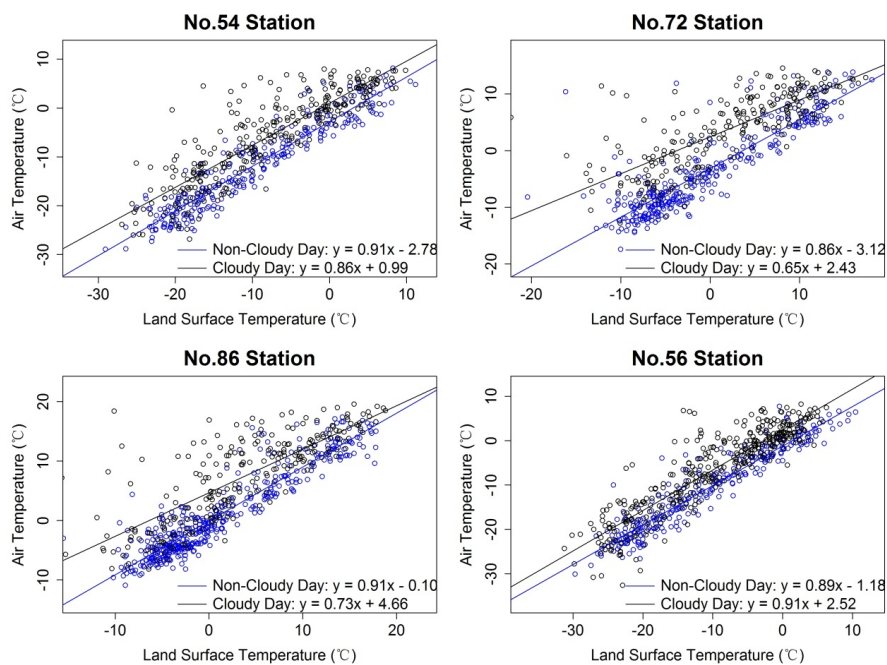
684

685

686 Figure 10: Comparisons of T_{\max} estimation accuracy between “cloudy day” and “non-cloudy day”

687 conditions at four meteorological stations presenting the largest decline in RMSE.

688



689

690

691 Figure 11: Comparisons of T_{\min} estimation accuracy between “cloudy day” and “non-cloudy day”

692 conditions at four meteorological stations presenting the largest decline in RMSE.

693

694